J|A|C|S
ARTICLES
Published on Web 11/23/2006

A Combined Quantum Mechanical and Molecular Mechanical Study of the Reaction Mechanism and α-Amino Acidity in Alanine Racemase

Dan Thomas Major and Jiali Gao*

Contribution from the Department of Chemistry and Supercomputing Institute, Digital Technology Center, University of Minnesota, Minneapolis, Minnesota 55455

Received August 31, 2006; E-mail: gao@chem.umn.edu

Abstract: Combined quantum mechanical/molecular mechanical simulations have been carried out to investigate the origin of the carbon acidity enhancement in the alanine racemization reaction catalyzed by alanine racemase (AlaR). The present study shows that the enhancement of carbon acidity of α-amino acids by the cofactor pyridoxal 5′-phosphate (PLP) with an unusual, unprotonated pyridine is mainly due to solvation effects, in contrast to the intrinsic electron-withdrawing stabilization by the pyridinium ion to form a quinonoid intermediate. Alanine racemase further lowers the α-proton acidity and provides an overall 14−17 kcal/mol transition-state stabilization. The second key finding of this study is that the mechanism of racemization of an alanine zwitterion in water is altered from an essentially concerted process to a stepwise reaction by formation of an external aldimine adduct with the PLP cofactor. Finally, we have used a centroid path integral method to determine the intrinsic kinetic isotope effects for the two proton abstraction reactions, which are somewhat greater than the experimental estimates.

Introduction

Alanine racemase (EC 5.1.1.1) is a pyridoxal 5′-phosphate (PLP)-dependent enzyme which catalyzes the interconversion of L- and D-alanine.[1−3] The latter is an essential component of the peptidoglycan layer of bacterial cell walls,[4] and the biosynthesis of D-Ala is unique to bacteria, making the enzyme alanine racemase (AlaR) an attractive target for antibacterial drug design.[5−7] Alanine racemase is a homodimer with 388 amino acids in each subunit, in which the PLP cofactor (Chart 1) is covalently linked to Lys39 through an internal Schiff base.[8] Being catalyzed by an amino acid racemase, the D- to L-Ala interconversion has an equilibrium constant of unity.[9−12] Biochemical studies suggest that the mechanism of alanine racemization follows a sequence of transformations.[9,13,14] The first major step involves the binding of L-Ala and formation of an external aldimine with the PLP cofactor (Ala-PLP) by displacing its internal Schiff base linkage to Lys39 (Scheme 1). Subsequently, Tyr265′ (prime indicates residues from the second subunit) abstracts the C_α proton of the L-Ala-PLP adduct, which is followed by reprotonation of the planar carbanion intermediate by Lys39 from the opposite side to yield the D-enantiomer.[9,15] Finally, Lys39 reconnects with the cofactor PLP, displacing D-Ala from covalent linkage to the cofactor. Dissociation of the product from the active site restores the catalytic cycle. Mutagenesis experiments and measurements of kinetic isotope effects indicate that the proton abstraction reaction is the rate-limiting step, or at least partially rate-limiting, compared to the product release step.[9] The two key catalytic residues, Tyr265′ and Lys39, are located on opposite sides of the PLP cofactor,[16] forming an acid and base pair, with their protonation states matched to enable sequential deprotonation followed by protonation.[13]

Chart 1. The External Aldimine Adduct (Ala-PLP) of L-Alanine and Pyridoxal 5′-Phosphate Cofactor in Alanine Racemase

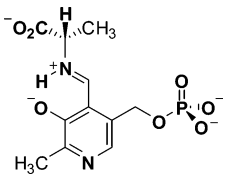

A key point in understanding the mechanism of the AlaR-catalyzed racemization is to elucidate the origin of the enhancement of the α-carbon acidity of the alanine substrate. Certainly,

(1) John, R. A. *Biochim. Biophys. Acta* **1995**, *1248*, 81−96.
(2) Eliot, A. C.; Kirsch, J. F. *Annu. Rev. Biochem.* **2004**, *73*, 383−415.
(3) Toney, M. D. *Arch. Biochem. Biophys.* **2005**, *433*, 279−287.
(4) Adams, E. *Adv. Enzymol. Relat. Areas Mol. Biol.* **1976**, *44*, 69−138.
(5) Mustata, G. I.; Soares, T. A.; Briggs, J. M. *Biopolymers* **2003**, *70*, 186−200.
(6) Mustata, G.; Briggs, J. M. *Protein Eng. Des. Sel.* **2004**, *17*, 223−234.
(7) Ondrechen, M. J.; Briggs, J. M.; McCammon, J. A. *J. Am. Chem. Soc.* **2001**, *123*, 2830−2834.
(8) Jansonius, J. N. *Curr. Opin. Struct. Biol.* **1998**, *8*, 759−769.
(9) Sun, S.; Toney, M. D. *Biochemistry* **1999**, *38*, 4058−4065.
(10) Watanabe, A.; Kurokawa, Y.; Yoshimura, T.; Kurihara, T.; Soda, K.; Esaki, N. *J. Biol. Chem.* **1999**, *274*, 4189−4194.
(11) Watanabe, A.; Kurokawa, Y.; Yoshimura, T.; Esaki, N. *J. Biochem.* **1999**, *125*, 987−990.
(12) Watanabe, A.; Yoshimura, T.; Mikami, B.; Esaki, N. *J. Biochem.* **1999**, *126*, 781−786.
(13) Spies, M. A.; Toney, M. D. *Biochemistry* **2003**, *42*, 5099−5107.
(14) Spies, M. A.; Woodward, J. J.; Watnik, M. R.; Toney, M. D. *J. Am. Chem. Soc.* **2004**, *126*, 7464−7475.
(15) Dixon, J. E.; Bruice, T. C. *Biochemistry* **1973**, *12*, 4762−4766.
(16) Watanabe, A.; Yoshimura, T.; Mikami, B.; Hayashi, H.; Kagamiyama, H.; Esaki, N. *J. Biol. Chem.* **2002**, *277*, 19166−19172.

Scheme 1. General Reaction Mechanism for Alanine Racemase

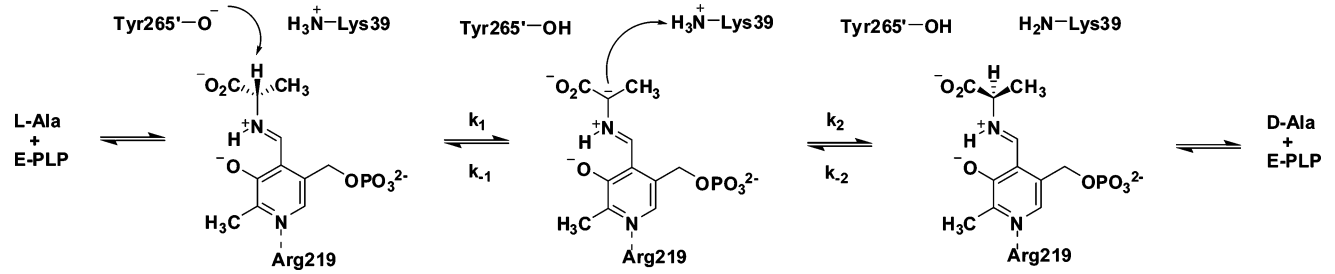

the formation of the Ala-PLP aldimine adduct plays a major role in increasing the α-carbon amino acidity in PLP-dependent enzymes. Typically, the pyridine nitrogen of PLP is protonated, making hydrogen-bonding interactions either with an anionic residue, such as Asp or Glu found in aminotransferases, or with a polar residue, Ser or Thr, in enzymes of the tryptophan synthase family.[2,3,8] The pyridinium ion of PLP acts as an effective electron sink, stabilizing the carbanion intermediate by forming a quinonoid species, which can be easily characterized by UV spectra.[9] However, alanine racemase is unique among the PLP-dependent enzymes in that the PLP pyridine is unprotonated. Ringe and co-workers first described the implication of this structural feature through analyses of X-ray crystal structures, which revealed that Arg219 directly donates a hydrogen bond to the pyridine nitrogen, preventing the formation of a cationic pyridinium ion (Figure 1).[17,18] This is further supported by the fact that the quinonoid intermediate was not observed in wild-type AlaR or in Arg219Gln and Arg219Ala mutants, whereas it is formed in the Arg219Glu mutant.[9] The last mutant, which is similar to other PLP-dependent enzymes in the pyridine binding site, can provide hydrogen-bonding stabilization to a protonated pyridine species. Significantly, despite the fact that the pyridine is unprotonated in AlaR, the apparent pK_a of the C_α proton in the Ala-PLP adduct is similar to those in other PLP-dependent enzymes, and AlaR is a proficient catalyst, accelerating the rate of proton abstraction by a factor of 10^{14} in comparison with the spontaneous deprotonation of an alanine zwitterion in water.[9,19,20,61] Thus, it is of great interest to understand the difference in the mechanism of carbon acidity enhancement by the PLP cofactor in enzymes that employ a protonated or an unprotonated pyridine. In this paper, we aim to elucidate the origin of the enormous catalytic power of alanine racemase and the unique features in carbon acidity enhancement through molecular dynamics (MD) simulations employing combined quantum mechanical and molecular mechanical (QM/MM) approaches.

The free energy reaction profile of the AlaR-catalyzed reaction was studied by Faraci and Walsh by measuring substrate and solvent deuterium isotope effects, and it was concluded that the transaldimination step is at least partially rate-limiting in the enzyme from *Bacillus stearothermophilus*.[21] Recently, the free energy reaction profile was further analyzed by Toney and co-workers, who optimized the individual rate constants for the entire catalytic cycle by matching the overall observed kinetic data obtained from various concentrations of the substrate and enzyme at different pH conditions.[14] From this analysis, it was found that the rate-limiting step is the proton abstraction step, and the primary kinetic isotope (KIE) effects, $^{H}k/^{D}k$, have been determined to be 1.9 and 1.3 for the L- to D-alanine and for the D- to L-alanine conversions, respectively.[13,21,22] The associated free energy barriers are 12.8 and 12.1 kcal/mol for the two proton-transfer steps in the enzyme. Spies and Toney identified a stable, common carbanion intermediate for the forward and reverse reactions, and this intermediate, which does not show the characteristic quinonoid spectrum, is at least 4 kcal/mol higher in free energy than the Michaelis complex of the external aldimine.[14] From the experimental K_M values for the binding of D- and L-alanine, Toney and co-workers estimated that the relative free energy between the two Michaelis complexes for the forward and reverse isomerizations is about 0.3 kcal/mol lower for the D-Ala-PLP complex. In other studies, a greater KIE of 5.4 was reported for the D-Ala C_α proton abstraction in the K39A AlaR mutant, where the small molecule methylamine was proposed to serve as the catalytic base, but it is likely to have raised the proton-transfer barrier to be truly rate-limiting.[10]

On the computational side, Briggs, McCammon, and co-workers have carried out a series of pK_a calculations,[7] MD simulations,[5,6] and structural modeling.[23] These studies focused on electrostatic, structural, and dynamical properties of the enzyme, with an emphasis for developing AlaR inhibitors. On the basis of electrostatic potential calculations, it was found that Tyr265′ is likely to be unprotonated, while Lys39 is protonated, and it was also suggested that Cys311′ is unprotonated.[7] Molecular dynamics simulations of the AlaR dimer with the two active sites occupied by the substrate and an inhibitor, respectively, indicated that the substrate is more tightly bound than the inhibitor.[5] Moreover, a specific water molecule in direct contact with the substrate or the inhibitor was identified,[5] along with a well-defined cluster of water molecules.[6] Bach et al. investigated the effect of PLP aldimine formation on the amino carbon acidity and concluded that the neighboring Schiff base is the primary reason for the enhanced C_α acidity in AlaR. However, none of the protonation states examined in their model systems correspond to that assumed for the AlaR reaction.[24] Thus, their results cannot be directly compared with the present study of alanine racemase catalysis. Toney performed semiempirical PM3 calculations on the decarboxylation of 2-aminoisobutyrate as a model for PLP-catalyzed decarboxylation reactions and found that both the Schiff base and pyridine ring

(17) Shaw, J. P.; Petsko, G. A.; Ringe, D. *Biochemistry* **1997**, *36*, 1329−1342.
(18) Morollo, A. A.; Petsko, G. A.; Ringe, D. *Biochemistry* **1999**, *38*, 3293−3301.
(19) Rios, A.; Crugeiras, J.; Amyes, T. L.; Richard, J. P. *J. Am. Chem. Soc.* **2001**, *123*, 7949−7950.
(20) Smith, G. G.; Reddy, G. V. *J. Org. Chem.* **1989**, *54*, 4529−4535.
(21) Faraci, W. S.; Walsh, C. T. *Biochemistry* **1988**, *27*, 3267−3276.
(22) Faraci, W. S.; Walsh, C. T. *Biochemistry* **1989**, *28*, 431−437.
(23) LeMagueres, P.; Im, H.; Ebalunode, J.; Strych, U.; Benedik, M. J.; Briggs, J. M.; Kohn, H.; Krause, K. L. *Biochemistry* **2005**, *44*, 1471−1481.
(24) Bach, R. D.; Canepa, C.; Glukhovtsev, M. N. *J. Am. Chem. Soc.* **1999**, *121*, 6542−6555.

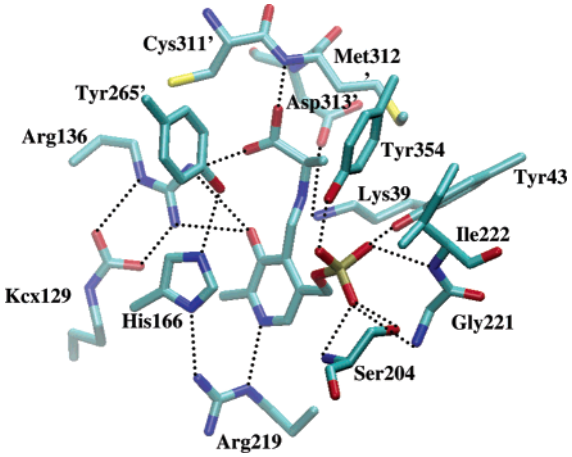

Figure 1. Active-site interactions of AlaR with the external aldimine adduct, Ala-PLP, from the X-ray crystal structure (PDB code 1L6G).

contribute to catalysis, with the former being more important.[25] Recently, we proposed that the amino carbon acidity enhancement of alanine in alanine racemase is a result of combined actions of solvent effects and enzyme stabilization of the carbanion, whereas the intrinsic charge delocalization upon forming a quinonoid intermediate is the dominant factor in typical pyridine-protonated PLP cofactor.[26]

In this paper, we report a detailed analysis of computational results of the alanine racemization reaction catalyzed by alanine racemase. An important goal is to gain an understanding of the unusual features of the PLP cofactor, which employs an unprotonated pyridine moiety to enhance the amino carbon acidity. Furthermore, we present computational evidence demonstrating that the rate enhancement in the catalyzed process results from combined effects of transition-state stabilization through differential hydrogen-bonding interactions in the active site and a change in the reaction mechanism from a concerted process in water to a stepwise reaction in the enzyme by forming the Ala-PLP aldimine adduct. We employ a combined classical mechanics and quantum mechanics potential to describe the chemical transformation, and we utilize a centroid path integral simulation method to account for nuclear quantum effects to determine the intrinsic kinetic isotope effects for the proton-transfer reactions. In the following, we first describe the computational procedures used in this study, followed by results and discussion. Finally, we highlight the major findings of this study.

Computational Details

A. Model for the Michaelis Complex of the External Aldimine and Alanine Racemase. A number of crystal structures of alanine racemase have been determined which show a fold belonging to the type III group of PLP-dependent enzymes.[8,16−18] AlaR is a homodimer, and each monomer contains two structural domains: (a) the N-terminal domain (residues 1−240), which forms an eight-stranded α/β barrel, and (b) the C-terminal domain (residues 241−388), which is characterized by a combination of α-helices and antiparallel β-sheets. The two subunits are arranged in an antiparallel fashion, with the two active sites positioned at the interface between the two monomers. Recently, Watanabe et al. reported two structures of AlaR at 2.0 Å,[16] in which AlaR is complexed respectively with the reaction intermediate analogues

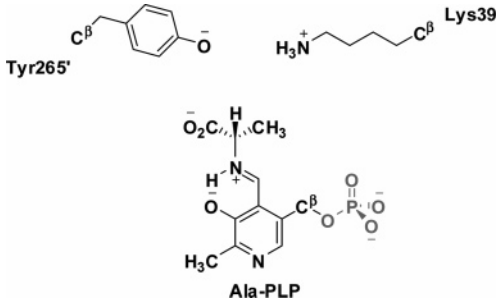

Figure 2. Schematic representation of the partition of quantum mechanics (black) and molecular mechanics (gray) regions in the simulation of the reactions catalyzed by alanine racemase. Boundary atoms are labeled C^{β}.

N-(5′-phosphopyridoxyl)-L-alanine and *N*-(5′-phosphopyridoxyl)-D-alanine. The latter structure was used to construct the external aldimine Michaelis complex in our study using the CHARMM program.[27] The protonation states of ionizable residues were assigned corresponding to pH 7. Thus, Glu and Asp residues are treated as anions and Lys and Arg as cations. Interior histidines are modeled as neutral residues, with the titratable hydrogen positioned at either the Nδ or Nϵ position, depending on hydrogen-bonding patterns with the surrounding amino acid residues. We have treated histidine residues that are exposed to the solvent or form ion-pairs as protonated. The protonation state of the Ala-PLP adduct is shown in Figure 2.

B. Combined SRP-QM/MM Potential Function. To model the rate-limiting proton-transfer reactions catalyzed by alanine racemase, we employed a combined quantum mechanical and molecular mechanical (QM/MM) potential[28,29] in molecular dynamic simulations. In this approach, the active site is represented explicitly by a QM model, and the remainder of the system is approximated by classical force fields. The QM region includes a fragment of the external aldimine adduct along with the specific acid and base residues, Lys39 and Tyr265′, resulting in a total of 58 atoms (Figure 2). The connections between the QM and MM regions, which consist of three sp^3 carbon atoms located at the two C_α atoms of Lys39 and Tyr265′ and the methylene group next to the phosphate moiety in PLP, are modeled by the generalized hybrid orbital (GHO) method.[30,31]

The QM model used in the present study follows the semiempirical Austin Model 1 (AM1)[32] formalism; however, we have re-parametrized the semiempirical model to generate a set of reaction-specific parameters (SRP)[33] for the alanine racemase reaction. Although it would be ideal to use ab initio molecular orbital theory or density functional theory (DFT) for the QM region, the computational costs are still intractable, and the semiempirical model enables us to carry out free energy simulations with sufficient sampling, essential for studying enzyme catalysis. The SRP-QM/MM potential provides a practical procedure for describing the electronic structure involving bond-breaking and bond-formation processes in enzymatic reactions. In the parametrization process, we have examined the structures and energies of model compounds (and the corresponding conjugate acids or bases) representing the catalytic residues Tyr265′ (phenol) and Lys39 (ethylamine), the external aldimine (Ala-PLP) excluding the phosphate moiety, and the alanine zwitterion by using ab initio molecular orbital and DFT

(25) Toney, M. D. *Biochemistry* **2001**, *40*, 1378−1384.
(26) Major, D. T.; Nam, K.; Gao, J. L. *J. Am. Chem. Soc.* **2006**, *128*, 8114−8115.
(27) Brooks, B. R.; Bruccoleri, R. E.; Olafson, B. D.; States, D. J.; Swaminathan, S.; Karplus, M. *J. Comput. Chem.* **1983**, *4*, 187−217.
(28) Gao, J. In *Reviews in Computational Chemistry*; Lipkowitz, K. B., Boyd, D. B., Eds.; VCH: New York, 1995; Vol. *7*, pp 119−185.
(29) Gao, J.; Thompson, M. A. *Combined Quantum Mechanical and Molecular Mechanical Methods*; American Chemical Society: Washington, DC, 1998; Vol. 712.
(30) Gao, J.; Amara, P.; Alhambra, C.; Field, M. J. *J. Phys. Chem. A* **1998**, *102*, 4714−4721.
(31) Amara, P.; Field, M. J.; Alhambra, C.; Gao, J. *Theor. Chem. Acc.* **2000**, *104*, 336−343.
(32) Dewar, M. J. S.; Zoebisch, E. G.; Healy, E. F.; Stewart, J. J. P. *J. Am. Chem. Soc.* **1985**, *107*, 3902−3909.
(33) Rossi, I.; Truhlar, D. G. *Chem. Phys. Lett.* **1995**, *233*, 231−236.

Table 1. Computed Proton Affinities (Enthalpies in kcal/mol) for the Conjugated Bases (B^-) Relevant to the Alanine Racemase Reaction in the Gas Phase

			mPW1PW91[a]		
acid (BH)	AM1	SRP-AM1	6-31+ G(d)	6-311++ G(3df,2p)	expt[b]
PhOH	347.0	350.6	345.8	350.1	350.5
$CH_3CH_2NH_3^+$	212.3	220.5	219.7	220.0	219.9
Ala (neutral)	350.7	371.6	370.6	370.7	
Ala (zwitterion)	358.4	382.0	380.9	381.5	
Ala-PLP	408.8	417.1	417.4	418.3	
Ala-PLP(H^+)	308.8	322.7	318.3	318.2	

[a] All geometries were optimized at the mPW1PW91/6-31+G(d) level of theory. [b] References 64 and 65.

Table 2. Computed Gas-Phase Basicities (Free Energies in kcal/mol) for the Conjugated Bases of BH[a]

acid (BH)	SRP-AM1	DFT	expt
PhOH	342.9	342.2	342.2[b]
$CH_3CH_2NH_3^+$	212.6	212.1	
Ala (neutral)	364.5	362.1	
Ala (zwitterion)	374.9	373.2	
Ala-PLP	409.2	409.2	
Ala-PLP(H^+)	313.9	308.6	

[a] DFT calculations employed mPW1PW91/6-311++G(3df,2p)//mPW1PW91/6-31+G(d). [b] Reference 64.

calculations, including MP2, MP4,[34] B3LYP,[35,36] and mPW1PW91[37] with the 6-31+G(d) basis set.[34] The best results were obtained at the mPW1PW91/6-311++G(3df,2p)//mPW1PW91/6-31+G(d) level of theory. The molecular properties used in the parametrization include the experimental heats of formation for phenol, ethylamine, and alanine. The values for the remaining compounds are not available experimentally, but they are obtained by using mPW1PW91/6-311++G(3df,2p) energy calculations along with zero-point energy and thermal corrections. In addition, the experimental or computed proton affinities for the respective conjugated bases are included. We have also considered geometrical variables (bond lengths and bond angles) and vibrational frequencies obtained at the mPW1PW91/6-31+G(d) level. To adequately describe the charge distribution in these molecules, we included the Mülliken population charges and molecular dipole moments (for the neutral species) in the penalty function for parameter optimization, although the charge restraints were used primarily to ensure balanced charge polarization rather than strictly fitting their values in view of the uncertainty in population analyses.

The nonlinear optimization of the SRP model follows a procedure described previously by York and co-workers,[38] starting with the original AM1 model as the initial input. Specifically, the core and resonance integrals, U_{ss}, U_{pp}, β_s, and β_p, are optimized first with allowed changes up to 1% from the original AM1 values. In the second step, the orbital exponents ζ_s, ζ_p and α parameters are included in the optimization (along with the parameters optimized in the previous step), also with a maximum change of 1% from the AM1. The subsequent step introduces the two-electron integral terms, G_{ss}, G_{sp}, G_{pp}, G_{p2}, and H_{sp}, followed by the Gaussian parameters L, M, and K. The latter parameters were constrained to 0.5% changes from the AM1 values, followed by a final fine-tuning step. Thus, the final SRP parameters for the alanine racemization reaction deviate only by a few percent from the original AM1 set, and such a careful parametrization protocol yields a highly accurate Hamiltonian that is comparable to mPW1PW91/6-311++G(3df,2p) calculations (Table 1; see also Supporting Information). Results of the model calculations are presented in Tables 1 and 2.

For the MM region, we used the CHARMM22 force field[39] for all protein atoms and the phosphate group in PLP, whereas the three-point charge TIP3P model was adopted for water molecules.[40] Although there are two active sites in the dimeric enzyme, we modeled the enzymatic process in the active site of the first subunit by the combined SRP-QM/MM potential. The external aldimine adduct in the second active site is located outside of the dynamical region of the system; for simplicity, we used standard van der Waals parameters from the CHARMM22 force field for analogous functional groups and the AM1 Mülliken population charges. X-ray structures reveal that Lys129 is carboxylated by a carbon dioxide to form a carbamate moiety (KCX residue).[16] A set of partial atomic charges was developed for the carbamate functional group, along with internal force field parameters assigned with values for similar molecular units in CHARMM. The interaction energies between a model KCX molecule and individual water molecules were calculated at the HF/6-31+G(d) level, and the partial atomic charges were fitted to reproduce the ab initio interaction energies. These results and the new KCX atom types and parameters are given as Supporting Information.

All ab initio and DFT calculations were done using the Gaussian 03 program.[41]

C. Free Energy Simulations. The classical potential of mean force (PMF) as a function of the reaction coordinate is defined as[42]

$$W_{CM}(z) = -RT \ln \rho(z) + C \quad (1)$$

where ρ is the probability density along the reaction coordinate z, R is the gas constant, T is the temperature, and C is a normalization constant. The reaction coordinate was defined as the difference between the breaking C_α−H bond and the forming O−H (Tyr265′ as base in the L-to-D conversion) or N−H (Lys39 as base in the D-to-L isomerization) bond. The PMF was obtained by employing adaptive umbrella-sampling molecular dynamics simulations.[42−44] In this approach, the reaction coordinate is divided into regions (windows) which are sampled in separate simulations. A biasing (umbrella) potential, $V_{bias}(z)$, was employed to improve the sampling of regions that are high in energy, yielding nearly uniform sampling of the potential energy surface (PES).[43] The biasing potential is ideally defined as $V_{bias}(z) = -W(z)$. In practice, a guess biasing potential is used first, which is subsequently improved as the PMF becomes more accurate. An additional harmonic restraint was added to the biasing potential along the reaction coordinate to focus the sampling of the PES in regions of interest. The free energies of the separate simulation windows along the reaction coordinate were combined by using the weighed histogram analysis method (WHAM) to remove the contributions of biasing potentials.[45]

Stochastic boundary conditions have been used in the present study to model the active site of alanine racemase.[46] The C_α atom of the Ala-PLP adduct was chosen as the center of the system, and the enzyme is embedded in a sphere of water molecules at a radius of 30 Å to mimic the aqueous environment. Water molecules that are within 2.6 Å of any non-hydrogen atom of the enzyme, substrate, and crystal water were deleted. All protein atoms outside of the 30 Å sphere were fixed

(34) Hehre, W. J.; Radom, L.; Schleyer, P. v. R.; Pople, J. A. *Ab Initio Molecular Orbital Theory*; John Wiley & Sons: New York, 1986.
(35) Becke, A. D. *Phys. Rev. A* **1993**, *98*, 5648−5652.
(36) Lee, C.; Yang, W.; Parr, R. G. *Phys. Rev. B* **1988**, *37*, 785−789.
(37) Adamo, C.; Barone, V. *J. Chem. Phys.* **1998**, *108*, 664−675.
(38) Giese, T. J.; Sherer, E. C.; Cramer, C. J.; York, D. M. *J. Chem. Theory Comput.* **2005**, *1*, 1275−1285.
(39) MacKerell, A. D., Jr.; et al. *J. Phys. Chem. B* **1998**, *102*, 3586−3616.
(40) Jorgensen, W. L.; Chandrasekhar, J.; Madura, J. D.; Impey, R. W.; Klein, M. L. *J. Chem. Phys.* **1983**, *79*, 926−935.
(41) Frisch, M. J.; et al. *Gaussian 03*, revision C.3; Gaussian, Inc.: Pittsburgh, PA, 2003.
(42) Kottalam, J.; Case, D. A. *J. Am. Chem. Soc.* **1988**, *110*, 7690−7697.
(43) Torrie, G. M.; Valleau, J. P. *J. Comput. Phys.* **1977**, *23*, 187−199.
(44) Hooft, R. W. W.; van Eijck, B. P.; Kroon, J. *J. Chem. Phys.* **1992**, *97*, 6690−6694.
(45) Kumar, S.; Bouzida, D.; Swendsen, R. H.; Kollman, P. A.; Rosenberg, J. M. *J. Comput. Chem.* **1992**, *13*, 1011−1021.
(46) Brooks, C. L., III; Brünger, A.; Karplus, M. *Biopolymers* **1985**, *24*, 843−865.

throughout the simulations. The dynamics for atoms in the range of 25−30 Å from the origin were propagated using the Langevin equation, and all atoms within 25 Å were treated by Newtonian molecular dynamics. In the Langevin region, the protein atoms were given a friction coefficient of 200 ps^{-1}, and it was set to 62 ps^{-1} for water molecules. The leapfrog integration scheme was used in all simulations with a time step of 1 fs, and the temperature of the system was set at 298 K.[47] The electrostatic forces were shifted to zero at 14 Å, while the van der Waals interaction energy was switched to zero from 12 to 14 Å. Bond lengths and bond angles involving hydrogen atoms were constrained using the SHAKE algorithm.[47]

To provide insights into enzyme catalysis, three reactions modeling the uncatalyzed and PLP-catalyzed reactions were investigated in aqueous solution for comparison. In these reactions, a phenoxide ion was used as the base, abstracting the C_α proton from Ala, Ala-PLP, and Ala-PLP(H^+) (Ala-PLP protonated at pyridine nitrogen), respectively. For simplicity, the phosphate moiety was not included in the Ala-PLP and Ala-PLP(H^+) model reactions. Periodic boundary conditions were used, and long-range electrostatic interactions were treated by the particle mesh Ewald method.[48] The center-of-mass of the reactant (QM subsystem) was placed at the center of a cubic box of dimensions $46.4 \times 46.4 \times 46.4$ $Å^3$. The solution-phase reactions were performed using the constant particle−temperature−pressure (NPT) ensemble at 298 K and 1 atm.[49]

Each system was slowly heated over the course of 25 ps, followed by 275 ps of equilibration. Thereafter, the two steps of the AlaR reaction were each divided into 13 windows, while the model reactions were divided into 31 windows each. Each window was equilibrated for 100 ps and sampled for ca. 100 ps. Thus, the total simulations lasted for a total of ca. 24 ns.

D. Computation of Kinetic Isotope Effects. The PMF obtained from classical MD simulations does not include nuclear quantum mechanical effects, which are required to compute kinetic isotope effects (KIEs). In the current work, we employ two complementary approaches, based on centroid path integral (PI) simulations[50,51] and the ensemble-averaged variational transition state theory with multidimensional tunneling (EA-VTST/MT),[52] to evaluate the quantum mechanical (QM) PMF for the alanine racemase reaction. In both methods, the QM rate constant, k_{QM}, is related to the classical rate constant by a quantum correction factor,

$$k_{QM} = \kappa k_{CM}^{TST} \tag{2}$$

where k_{CM}^{TST} is the transition state theory rate constant derived from the classical mechanical (CM) PMF, and κ is the quantum correction factor, which is defined as follows:

$$\kappa = \frac{k_{QM}}{k_{CM}^{TST}} = \exp[-(\Delta G_{QM}^{\ddagger} - \Delta G_{TST}^{\ddagger})/RT] \tag{3}$$

where $\Delta G_{QM}^{\ddagger}$ and $\Delta G_{TST}^{\ddagger}$ are the QM and CM (TST) free energies of activation.

In the centroid PI simulation, we represent each quantized atom by a ring of particles or beads whose geometrical center (centroid) is constrained to its classical position. Thus, for each classical configuration sampled in MD umbrella-sampling simulations, we perform PI sampling to obtain the QM correction for nuclear motions. When the PI calculations are performed along the reaction coordinate, we obtain a QM correction at each point of the reaction coordinate, resulting in a QM PMF as a function of the centroid coordinate. The method differs from centroid molecular dynamics[53,54] in that MD simulations are performed classically, followed by PI simulation corrections, and it provides an efficient procedure to approximate quantum effects. This approach was first used by Sprik et al.[55] and has been exploited by Hwang et al. for chemical reactions.[56] Hwang et al. called this approach the quantized classical path (QCP) method. We have implemented a bisection sampling technique,[50,51,57] which greatly improves the convergence of PI calculations.

The key feature of the bisection quantized classical path (BQCP) approach is the use of double averaging of configurations from CM molecular dynamics simulations and configurations of free particle distributions for the quantized particles in PI simulations. Specifically, the quantum correction factor is computed as follows:

$$\kappa(\bar{x}) = \exp[-(\Delta G_{QM}(\bar{x}) - \Delta G_{CM}(\bar{x}))/RT] = \left\langle \left\langle \exp\left[-\frac{1}{RT}\frac{1}{P}\sum_{k}^{P} \Delta U_k \right] \right\rangle_{FP,\bar{x}} \right\rangle_{U(\bar{x})} \tag{4}$$

where P is the number of beads and $\Delta U_k = U(x_k) - U(\bar{x})$ is the difference in potential energy between bead k at x_k and the classical (centroid) position x. In eq 4, the outer average, $\langle \cdots \rangle_{U(\bar{x})}$, is over CM simulations using the potential $U(\bar{x})$. The inner average, $\langle \cdots \rangle_{FP,\bar{x}}$, is over the free particle distribution of quantized particles. In the bisection sampling scheme, we have taken advantage of the fact that the free particle distribution is known exactly and PI configurations can be sampled completely independently, which enhances the convergence of PI averaging.[50,51,57] Furthermore, we have developed a perturbation scheme for computing the free energy difference resulting from isotope substitutions, which gives the accuracy needed for computing KIEs.[58]

In the present study, we used 32 beads for each of the three quantized atoms (donor and acceptor heavy atoms plus the proton) involved directly in the proton transfer for the reaction in alanine racemase. Previous studies have shown that this treatment yields good convergence in the overall quantum corrections for modeling proton-transfer reactions in water.[51] BQCP simulations were performed on classical configurations along the PMF reaction coordinate, taken from simulations roughly corresponding to the reactant state (R), transition state (TS), and product state (P) windows for the proton-transfer reactions in the active site of AlaR. About 15 000 configurations were extracted from the MD trajectory, each of which was sampled by 10 free particle distributions to enumerate the quantum corrections. The QM correction along the entire reaction path was represented by a fitted inverse asymmetric Eckart potential via nonlinear Levenberg−Marquardt minimization. The BQCP method has been implemented in CHARMM.

The computational procedure for the EA-VTST/MT method has been described in detail in two recent review articles.[59,60] Thus, we only outline the specific details used in the present calculation. The quantum correction factor was obtained via a two-stage procedure. In stage 1, we chose approximately 300 configurations at the R, TS, and P regions to obtain the corrections due to quantization of bound vibrations using instantaneous normal-mode analysis. In this step, the degree of freedom corresponding to the reaction coordinate has been excluded by a

(47) Allen, M. P.; Tildesley, D. J. *Computer Simulation of Liquids*; Oxford University Press: Oxford, U.K., 1987.
(48) (a) Darden, T.; York, D. M.; Pedersen, I. *J. Chem. Phys.* **1993**, *98*, 10089−10092. (b) Nam, K.; Gao, J.; York, D. M. *J. Chem. Theory Comput.* **2005**, *1*, 2−13.
(49) Feller, S. E.; Zhang, Y.; Pastor, R. W.; Brooks, B. R. *J. Chem. Phys.* **1995**, *103*, 4613−4621.
(50) Major, D. T.; Gao, J. *J. Mol. Graphics Modell.* **2005**, *24*, 121−127.
(51) Major, D. T.; Garcia-Viloca, M.; Gao, J. *J. Chem. Theory Comput.* **2006**, *2*, 236−245.
(52) Alhambra, C.; Corchado, J.; Sánchez, M. L.; Garcia-Viloca, M.; Gao, J.; Truhlar, D. G. *J. Phys. Chem. B* **2001**, *105*, 11326−11340.
(53) Gillan, M. J. *J. Phys. C: Solid State Phys.* **1987**, *20*, 3621−3641.
(54) Voth, G. A. *Adv. Chem. Phys.* **1996**, *93*, 135−218.
(55) Sprik, M.; Klein, M. L.; Chandler, D. *Phys. Rev. B: Condens. Matter Mater. Phys.* **1985**, *31*, 4234−4244.
(56) Hwang, J. K.; Chu, Z. T.; Yadav, A.; Warshel, A. *J. Phys. Chem.* **1991**, *95*, 8445−8448.
(57) Pollock, E. L.; Ceperley, D. M. *Phys. Rev. B: Condens. Matter Mater. Phys.* **1984**, *30*, 2555−2568.
(58) Major, D. T.; Gao, J. Manuscript in preparation.
(59) Gao, J.; Truhlar, D. G. *Annu. Rev. Phys. Chem.* **2002**, *53*, 467−505.
(60) Pu, J.; Gao, J.; Truhlar, D. G. *Chem. Rev.* **2006**, *106*, 3140−3169.

projection operator, and the PMF in stage 1 is called the quasiclassical PMF. In stage 2, we include quantum tunneling contributions for the degree of freedom of the reaction coordinate by averaging over reaction trajectories optimized using the structures of the transition-state ensemble from classical umbrella-sampling simulations. To make the trajectory computations tractable, we used 10 transition structures for averaging. In the EA-VTST/MT calculations, a total of 40 atoms were included in the instantaneous normal-mode calculations for the L→D reaction, and 38 atoms for the D→L reaction.

Results and Discussion

A. Enhancement of α-Amino Carbon Acidity by PLP Cofactor in Alanine Racemase. The alanine racemization by AlaR involves two proton abstraction reactions at the α-amino carbon by two weak bases, an unprotonated Tyr residue in the L-to-D conversion, and a neutral Lys residue in the D-to-L isomerization. In aqueous solution, the pK_a of the carbon acidity for a zwitterionic amino acid such as Gly is 28.9,[61] while the pK_a's for phenol and ethylammonium ion, representing the side chains of Tyr and Lys, are 10.0[62] and 10.8,[63] respectively. Given that the pK_a of Tyr265′ in AlaR is lowered to 7.3,[9] the enzyme still must overcome a huge pK_a mismatch in both the forward and reverse conversions of alanine between the two enantiomers. The formation of the aldimine adduct between the substrate and the cofactor pyridoxal 5′-phosphate provides a key mechanism for the enhanced carbon acidity. Interestingly, the pyridine nitrogen is typically protonated, denoted as Ala-PLP(H^+), in PLP-dependent enzymes, but alanine racemase is unique in that the pyridine moiety is unprotonated (specified as Ala-PLP in the following discussion) and acts as a hydrogen-bond acceptor from Arg219 (Figure 1).[3,8,16−18] Two factors contribute to the increase in the carbon acidity in the Ala-PLP(H^+) adduct. First, the presence of the protonated Schiff base greatly stabilizes the neighboring carbanion after proton abstraction.[24,25] This is supported by the finding of Richard and coworkers that the acidity constant of the α-amino carbon acid is dramatically increased, by a factor of 10^7, by addition of acetone to form an iminium ion.[19] The second factor responsible for increasing the carbon acidity by Ala-PLP(H^+) is the delocalization of the anionic charge into the protonated pyridine ring, which acts as an electron sink, to form a quinonoid intermediate. Experimentally, this intermediate can be conveniently detected by the appearance of a band at ca. 500 nm in the UV absorption spectrum. However, in AlaR, the charge delocalization stabilization is absent, at least spectroscopically, as the quinonoid moiety was not detected in wild-type enzyme and mutants that lack hydrogen-bond-accepting abilities.[9] Yet, the proton abstraction reaction catalyzed by AlaR is as efficient as other PLP-dependent enzymatic reactions. A major goal of this study is to elucidate the difference in α-amino acidity enhancement by alanine racemase that employs an unprotonated pyridine in the external aldimine, Ala-PLP, as compared to that by Ala-PLP-(H^+) in other PLP-dependent enzymes.

To accomplish this goal, we first sought to determine the gas-phase proton affinities and basicities for a series of compounds and their conjugated acids, representing the Tyr and Lys residues, the neutral and zwitterionic forms of alanine, and the N-protonated and unprotonated Ala-PLP adduct excluding the phosphate group (representing the external aldimine) (Chart 1). The gas-phase properties provide information on the intrinsic acidities of these compounds in the absence of solvent and enzyme effects. Furthermore, we use the experimental and computational gas-phase proton affinities to optimize a set of specific reaction parameters (SRP)[33] within the semiempirical AM1 formalism.[32] Table 1 lists proton affinities computed using semiempirical AM1 and SRP-AM1 models, mPW1PW91/6-31+G(d), and mPW1PW91/6-311++G(3df,2p) DFT calculations, both employing the mPW1PW91/6-31+G(d) optimized geometries. Table 2 gives the computed gas-phase basicities, which are the standard-state free energy changes for the deprotonation of the conjugated acid in the gas phase. In Table 3, we present the free energies of the proton abstraction reactions of the neutral and zwitterionic forms of alanine and the pyridine-protonated and unprotonated external aldimine adducts with a phenolate anion in aqueous solution. The proton abstraction by a phenolate ion may be considered as a model reaction in water for the corresponding enzymatic reaction for the L- to D-alanine conversion.

Table 3. Computed Free Energies of Reaction (kcal/mol) for the Proton Abstraction of Acids BH by Phenolate Ion (PhO^-) in the Gas Phase and in Solution and for the Reaction in Alanine Racemase (AlaR)

$BH + PhO^- \rightarrow B^- + PhOH$

		aqueous phase	
acid (BH)	gas phase[a]	MD (PMF)	expt
Ala (neutral)	19.9		
Ala (zwitterion)	31.0	30.9	25.8[b]
Ala-PLP(H^+)	−33.6	1.3	2.7[d]
Ala-PLP	67.0	12.7	>8.2[b]
Ala-PLP in AlaR		6.6	>4.2[c]

[a] mPW1PW91/6-311++G(3df,2p)//mPW1PW91/6-31+G(d). [b] Reference 61. [c] Reference 14. [d] Reference 15.

The experimental proton affinities are available for phenolate ion[64] and for $EtNH_2$[65] which are 350.5 and 219.9 kcal/mol, respectively, and provide validation of the methods used in the calculations. Although results from different levels of molecular orbital and density functional theory are all reasonable, the mPW1PW91/6-311++G(3df,2p) method yields the best agreement with experiment. Thus, it is used for compounds that do not have experimental data for the SRP parametrization, and results from this method are also used in the discussions throughout this paper. Note that the original AM1 model underestimates the experimental or DFT proton affinities in the range of 3.5 kcal/mol for phenolate ion to 23 kcal/mol for alanine zwitterion, with a mean unsigned error (MUE) of 12.0 kcal/mol. By slight readjustment of the AM1 parameters, we obtained an SRP-AM1 model that yields gas-phase proton affinities in excellent agreement with the available experimental data and mPW1PW91 results. The MUE by the SRP model is only 1.5 kcal/mol in comparison with the DFT results. The MUE excluding Ala-PLP(H^+) (which was not include in the parametrization) is 0.9 kcal/mol. The computed gas-phase basicities for phenolate ion and ethylamine reported in Table 2 are also in good accord with experiment, from both the DFT and SRP-AM1 models. Overall, the gas-phase basicities are about 7−10

(61) Rios, A.; Amyes, T. L.; Richard, J. P. *J. Am. Chem. Soc.* **2000**, *122*, 9373−9385.
(62) Jaffe, H. H. *Chem. Rev.* **1953**, *53*, 199.
(63) Segel, I. H. *Biochemical Calculations*; John Wiley & Sons: New York, 1976.
(64) DeTuri, V. F.; Ervin, K. M. *Int. J. Mass Spectrom.* **1998**, *175*, 123−132.
(65) Hunter, E. P.; Lias, S. G. *J. Phys. Chem. Ref. Data* **1998**, *27*, 413−656.

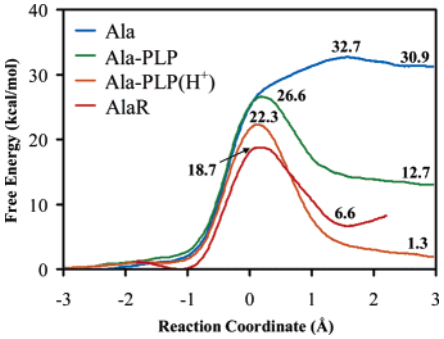

Figure 3. Computed classical potentials of mean force for proton abstraction reactions of alanine and a phenoxide ion in various forms: blue, alanine zwitterion; green, Ala-PLP; and orange, Ala-PLP(H^+) all in water; and red, Ala-PLP in alanine racemase.

kcal/mol smaller than the corresponding proton affinities due to the inclusion of the entropy correction.

The relative free energies and pK_a values were obtained by a series of MD simulations employing umbrella sampling for the proton abstraction reactions of alanine zwitterion, the external aldimine adduct Ala-PLP, and Ala-PLP(H^+) with a phenolate ion in water. Furthermore, the calculations provided validation of the potential energy functions and free energy simulation methods used in the enzymatic reactions. These reactions represent a model for the enzymatic process in the L- to D-alanine conversion, which is initiated by a proton transfer from the α-amino carbon to the Tyr265′ phenolate anion. The reaction of alanine zwitterion with PhO^- provides the reference reaction without the effects of cofactor and the enzyme, while the two reactions of the external aldimine species examine the difference between a protonated pyridine and an unprotonated pyridine in the PLP cofactor. The computed free energy profiles in water as well as that for the proton abstraction of Ala-PLP by Tyr265′ in alanine racemase are shown in Figure 3, and the results are summarized in Table 3.

For the uncatalyzed deprotonation of alanine by phenolate ion in water, we obtained a free energy of 30.9 kcal/mol using the SRP-AM1 potential, which is about 5 kcal/mol greater than the experimentally determined value (25.8 kcal/mol) based on pK_a values for glycine and phenol. The computed pK_a for Ala, based on the PMF and the experimental value for phenol, is 32.7, comparable to a value of 28.9 for Gly.[61] In comparison with the gas-phase results, there is a relatively small solvent effect. Figure 3 shows that spontaneous proton exchange is extremely disfavored thermodynamically in aqueous solution at 25 °C, and a carbanion species is unlikely to exist in water, but the reaction becomes feasible upon formation of the external aldimine species with the pyridoxal cofactor. Figure 3 shows a computed free energy of reaction of ca. 1 kcal/mol for the C_α proton abstraction by PhO^-, which translates to an estimated pK_a of 11.0 for Ala-PLP(H^+). This may be compared with an early experimental estimate of 12 by Bruice et al., based on extrapolation from related experiments.[15] Importantly, both experiment and computation indicate major enhancement of carbon acidity of alanine by the PLP cofactor. The deviation between computational and experimental results in Table 3 is mainly due to an overestimate of the solvation effects on the ionization of alanine zwitterion and an underestimate of the reaction free energy of Ala-PLP(H^+) in Figure 3.

Without protonation at the pyridine nitrogen of the PLP cofactor, we obtained a free energy of proton abstraction of 12.7 kcal/mol, which corresponds to a predicted pK_a of 19.3 for the α-amino carbon in Ala-PLP. There is no experimental data for direct comparison in this case because, under these conditions, either the pyridine nitrogen would be protonated or the Schiff base would be deprotonated. Nevertheless, it is expected that the free energy of deprotonation would be more endoergonic for Ala-PLP than for the reaction of Ala-PLP(H^+) because of the difference in their intrinsic stabilities. Thus, the computed PMF for the proton abstraction of the Ala-PLP by a phenoxide ion is reasonable (Figure 3). Significantly, the unprotonated PLP cofactor (at the pyridine nitrogen) can also significantly enhance the carbon acidity of α-amino acid in water, by as much as 13 pK_a units. By comparing the computed free energies of reaction for the two aldimine species in water (Figure 3), we find that the charge delocalization effect of the protonated pyridine ring further lowers the carbon acidity by 8 pK_a units (11 kcal/mol) in Ala-PLP(H^+).

Interestingly, the origins of the carbon acidity enhancement by Ala-PLP and by Ala-PLP(H^+) are different in aqueous solution. First, we consider the intrinsic properties of these compounds in the gas phase. Table 2 shows that the computed gas-phase basicity (free energy) of the conjugated base of Ala-PLP(H^+) is significantly smaller than that of the alanine zwitterion. Thus, the formation of the pyridine-protonated aldimine species, Ala-PLP(H^+), intrinsically increases the α-amino acidity by −65 kcal/mol. However, the formation of Ala-PLP has the opposite effect, reducing the carbon acidity by 36 kcal/mol. These findings are in good accord with the proposal that a protonated pyridine ring acts as an electron sink to stabilize the carbanion base. We then examined solvation effects in aqueous solution (Table 3) by comparing the estimated pK_a from free energy simulations presented in Figure 3. Remarkably, there is a major "leveling effect" for the two aldimine species, Ala-PLP and Ala-PLP(H^+), by aqueous solvation, resulting in a computed pK_a of 19.3 and 11.0, respectively. This represents only about 11 kcal/mol difference as a result of strong solvent stabilization (−54 kcal/mol) of the conjugated base of Ala-PLP and solvent destabilization (+35 kcal/mol) of the conjugated base of Ala-PLP(H^+), which may be contrasted with the remarkable difference of 101 kcal/mol in the gas phase. These results demonstrate that the origins of carbon acidity enhancement are different in the two forms of external aldimine adduct. In Ala-PLP(H^+), the carbon acidity is due to the intrinsic ability of the protonated Schiff base and the protonated pyridine ring, acting as an electron sink, to stabilize the carbanion intermediate with the formation of a quinonoid intermediate. On the other hand, solvation effects strongly stabilize the more charge-localized conjugated base of Ala-PLP.

In the enzyme alanine racemase, ion-pair and hydrogen-bonding interactions with residues in the active site further stabilize the conjugated base of the external aldimine Ala-PLP by about 6 kcal/mol relative to the aqueous process. Using the pK_a (7.3) of Tyr265′ in AlaR,[9] which is smaller than the pK_a of phenol in water (10.0), we estimate that the pK_a of the Ala-PLP adduct is 12.2 in the active site of alanine racemase. The quantitative contributions of specific residues will be discussed below.

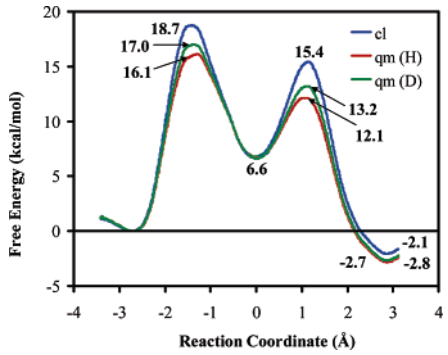

Figure 4. Computed classical and quantum mechanical potentials of mean force for the proton and deuteron abstraction of Ala-PLP by Tyr265′, and the reprotonation of Ala-PLP carbanion intermediate by Lys39 in alanine racemase.

B. Potential of Mean Force for the Alanine Racemase Reaction. The computed classical and quantum mechanical potentials of mean force for the alanine racemization reaction, for both proton transfer and deuteron transfer, catalyzed by AlaR, are depicted in Figure 4. The AlaR catalytic cycle involves two proton-transfer reactions in each direction of the racemization. In the L-to-D direction, the Tyr265′ phenolate ion abstracts the C_α proton to yield a carbonanion intermediate, which is followed by a proton transfer from Lys39 to form D-alanine (Scheme 1). The reaction coordinate for the first proton-transfer step is defined as the difference in bond length between $C_\alpha\cdots H$ and $H\cdots O_{Tyr}$, i.e., $R_C^1 = R(C_\alpha-H) - R(H-O_{Tyr})$. Similarly, the reaction coordinate for the second proton-transfer step is defined as the difference between $N_{Lys}\cdots H$ and $H\cdots C_\alpha$, i.e., $R_C^2 = R(N_{Lys}-H) - R(H-C_\alpha)$. By this definition, the Ala-PLP carbanion intermediate has a reaction coordinate that is positive in the first step and negative in the second step. In constructing Figure 4, we shifted the reaction coordinate by -1 and $+1$ Å for the first and the second reaction steps, respectively, in order to illustrate both reaction profiles in the same figure. Furthermore, we set the relative free energy of the reactant-state minimum of the L-Ala-PLP enzyme complex as zero and the free energies for the Ala-PLP deprotonation intermediate to be identical for both reaction steps. This results in an overall free energy of reaction of -2.8 kcal/mol for the conversion from L- to D-alanine. However, it should be noted that one shall not use this free energy difference to compute the equilibrium constant for comparison with experiment because the anchoring of free energy at the reaction intermediate for the two proton-transfer steps is somewhat arbitrary, since the definitions of the reaction coordinate are different. To make a rigorous connection to define the relative free energies, we have to construct a two-dimensional free energy surface for R_C^1 and R_C^2, and this would significantly increase the computational costs. It is, nevertheless, interesting to notice that the relative energies of the L- and D-Ala-PLP complex are close. Alternatively, we could have simply placed the free energy of the D-Ala-PLP complex at the value (-0.3 kcal/mol) derived from the experimental equilibrium constant.[14]

The PMF for the AlaR reaction is in good qualitative agreement with the free energy reaction profile deduced from experimental kinetic data by Toney and co-workers.[14] The key features of Figure 4 demonstrate that the alanine racemization undergoes a stepwise mechanism, evidenced by the presence of a stable Ala-PLP carbanion intermediate. Experimental studies placed a lower limit of >4.2 kcal/mol in free energy above the external aldimine complex, based on spectroscopic sensitivity for the absence of a quinonoid moiety,[14] which may be compared with our computational estimate of 6.6 kcal/mol. Significantly, this intermediate is generally believed to be a low-energy species in typical PLP-dependent enzymes due to the formation of a quinonoid intermediate. In AlaR, the lack of protonation of the pyridine ring prevents effective charge delocalization, raising the relative free energy of this intermediate.[3] A second feature of the reaction profile in Figure 4 is the change in reaction mechanism in comparison with the alanine zwitterion racemization in water (Figure 3). Without the PLP cofactor, the carbanion species is extremely unstable (Figure 3), and in fact, the reprotonation is expected to be concerted with the proton abstraction process.[61] The formation of the external aldimine adduct stabilizes the carbanion, accompanied by a lowering of the $C_\alpha H$ pK_a by 13 units from computation, in accord with experimental estimates.[14,15] The enzyme AlaR further stabilizes this intermediate species by 6.1 kcal/mol, yielding an estimated pK_a of 12.2 for the Ala-PLP external aldimine in the enzyme (the experimental pK_a of 7.3 for Tyr265′ was used as reference).[9]

Quantitatively, the computed free energy of activation for the proton abstraction by Tyr265′ phenolate ion is 16.1 kcal/mol, which may be compared with the experimental value of 12.8 kcal/mol.[14] The agreement with experiment is good, considering the computational complexity involved in the enzymatic process. There is a small free energy barrier of 5.5 kcal/mol for the reprotonation by Lys39. If we consider the reverse reaction, i.e., D-to-L conversion, which involves a proton abstraction of the Ala-PLP aldimine by a neutral Lys39, the computed free energy barrier is 14.9 kcal/mol to yield the same deprotonation intermediate, also in rough agreement with experiment (12.5 kcal/mol). We point out that the CM potentials of mean force gave barriers of 18.7 kcal/mol for the Tyr265′ proton abstraction and 17.5 kcal/mol for the Lys39 proton abstraction, which are both 2.6 kcal/mol higher than the values obtained from the potentials of mean force that include the nuclear QM effects. This reinforces previous conclusions that zero-point effects and QM tunneling, which are both included in the present PI simulations (Figure 4), are important for computing rate constants for enzymatic reactions involving hydrogen transfers, and the trends observed here are consistent with previous findings.[59,66,67]

Note that the distances between the proton donor and acceptor atoms become significantly shorter at the transition state in both reaction steps, with values of 2.6 and 2.7 Å (Tables 4 and 5), which may be compared to average distances of about 3.2 Å in the external aldimine complexes and the Ala-PLP carbanion intermediate state (Figure 5). Similar features have been found in other proton- or hydride-transfer reactions in a number of enzymes, and sometimes this feature has been described as a dynamical gating mechanism.[68−70]

Watanabe et al. suggested a variation of the mechanism investigated here.[16] In this discussion, the racemization reaction

(66) Billeter, S. R.; Webb, S. P.; Agarwal, P. K.; Iordanov, T.; Hammes-Schiffer, S. *J. Am. Chem. Soc.* **2001**, *123*, 11262−11272.
(67) Hwang, J. K.; Warshel, A. *J. Am. Chem. Soc.* **1996**, *118*, 11745−11751.
(68) Liang, Z. X.; Klinman, J. P. *Curr. Opin. Struct. Biol.* **2004**, *14*, 648−655.
(69) Benkovic, S. J.; Hammes-Schiffer, S. *Science* **2003**, *301*, 1196−1202.
(70) Garcia-Viloca, M.; Alhambra, C.; Truhlar, D. G.; Gao, J. L. *J. Comput. Chem.* **2003**, *24*, 177−190.

Table 4. Average Distances for Selected Hydrogen-Bonding Interactions in the Michaelis Complex Reactant State, the Transition State, and the Deprotonation Intermediate State in the Proton Transfer from the L-Ala-PLP Substrate to Tyr265′[a]

		distance		
donor	acceptor	reactant state	transition state	intermediate state
NE, Arg219	N1, PLP	2.56	2.53	2.52
NH1, Arg219	ND1, His166	2.92	3.04	3.03
NH1, Arg136	O3A, PLP	2.94	2.84	2.73
NH2, Arg136	O3A, PLP	2.74	2.64	2.71
NH1, Arg136	OXT, PLP	2.71	3.10	2.64
NE2, His 166	OH, Tyr265′	2.88	2.88	3.13
OH2, Wat-f	OH, Tyr265′	2.90	2.96	3.25
OH2, Wat-f	OP2, PLP	2.62	2.78	2.65
N, Met312′	O, PLP	2.81	2.67	2.83
NZ, Lys39	OD2, Asp313′	2.65	2.67	2.69
NZ, Lys39	OH, Tyr43	2.95	2.95	3.08
CA, PLP	OH, Tyr265′	3.20	2.58	3.24
HA, PLP	OH, Tyr265′	2.16	1.20	0.99
CA, PLP	HA, PLP	1.14	1.43	2.40

[a] All distances are given in angstroms and have been averaged over 5000 configurations. Standard deviations in the average distances are 0.1−0.3 Å.

Table 5. Average Distances for Selected Hydrogen-Bonding Interactions in the Michaelis Complex Reactant State, the Transition State, and the Deprotonation Intermediate State in the Proton Transfer from the D-Ala-PLP Substrate to Lys39[a]

donor	acceptor	reactant state	transition state	intermediate state
NE, Arg219	N1, PLP	2.56	2.53	2.51
NH1, Arg219	ND1, His166	2.93	3.00	3.01
NH1, Arg136	O3A, PLP	2.71	2.66	2.71
NH2, Arg136	O3A, PLP	2.69	2.67	2.74
NH1, Arg136	OXT, PLP	2.67	2.53	2.65
NE2, His 166	OH, Tyr265′	3.94	3.95	2.68
OH, Tyr265′	OXT, PLP	3.02	3.19	3.37
OH2, Wat-f	OP2, PLP	2.72	2.72	2.62
N, Met312′	O, PLP	2.84	2.91	2.69
NZ, Lys39	OD2, Asp313′	2.83	2.74	2.58
NZ, Lys39	OH, Tyr43	4.15	4.41	4.70
CA, PLP	NZ, Lys39	3.18	2.72	3.19
HA, PLP	NZ, Lys39	2.14	1.37	1.02
CA, PLP	HA, PLP	1.15	1.37	2.24

[a] All distances are given in angstroms and have been averaged over 5000 configurations. Standard deviations in the average distances are 0.1−0.3 Å.

is coupled to a sequence of proton shuffling between the Tyr265′ and Lys39 via the carboxylate group of the external aldimine substrate. It was suggested that Tyr265′, following proton abstraction from Ala-PLP, transfers its proton to the carboxylate group of the planar Ala-PLP intermediate, which in turn delivers the proton to Lys39. We have examined this possibility in our computations, but we found that Tyr265′ was never correctly oriented to allow proton transfer to the proposed carboxylate group. In addition, it would require a full 180° rotation of the carboxylate group to point toward Lys39. The internal rotation of the hydroxyl group of acetic acid in water has a barrier of 15 kcal/mol,[71] and it is further hindered by hydrogen-bonding interactions with the backbone amide group of Met312′ and with Arg136 in the active site.

McCammon et al. investigated the protonation state of various amino acid residues in the active site as well as the cofactor.[7]

(71) Gao, J. L.; Pavelites, J. J. *J. Am. Chem. Soc.* **1992**, *114*, 1912−1914.

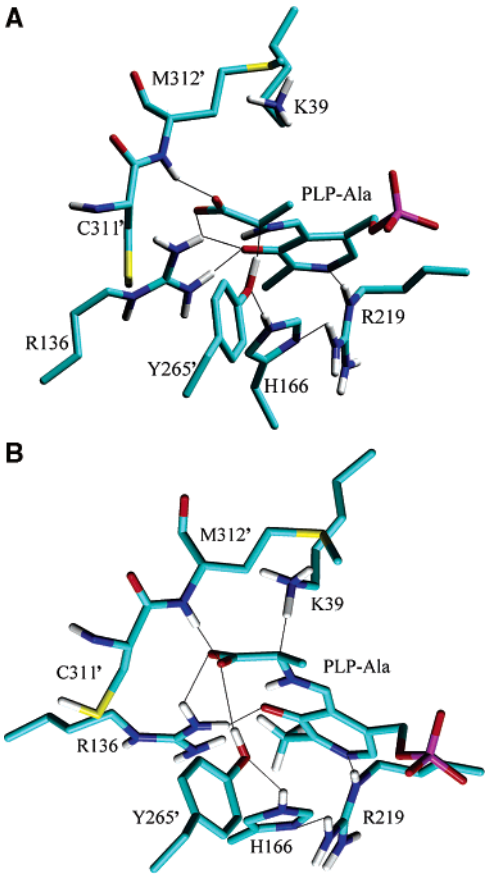

Figure 5. Representative transition-state structures for the proton abstraction by Tyr265′ (A) and the reprotonation by Lys39 (B) in alanine racemase.

In particular, it was suggested that Cys311′ could be deprotonated according to the calculated pK_a of this residue using a combined Poisson−Boltzmann and Monte Carlo strategy.[7] We have tested this possibility by utilizing a Cys311′ thiolate anion in the simulation, and we found that there is little effect on the free energy profile. Thus, the protonation state of Cys311′ does not affect the energetics of the proton abstraction reaction. We have also considered the possibility of a proton-transfer reaction between Arg219 and the pyridine nitrogen in PLP cofactor; however, the large pK_a difference (12 vs 5) between the two species likely makes it energetically disfavored, although we did not explicitly explore this. Furthermore, we have assigned the protonation pattern of the Schiff base and 3-hydroxyl group of the Ala-PLP aldimine as an internal ion-pair, consistent with experimental results.[72] In our studies of enzymatic reactions, we do not use restrainting potentials in any part of the system, including the cofactor. Although the PLP cofactor is treated quantum mechanically, allowing internal proton transfer to occur, the internal ion-pair remains stable throughout the simulations. To ascertain that the computational results are not influenced by the specific computational protocol used, we have examined different hydration schemes and sizes, used different and longer nonbonded cutoff distance, and varied the partial atomic charges of the phosphate group in the PLP cofactor. These tests showed that the changes in the computed PMF are within the statistical uncertainties of about 1−2 kcal/mol.

(72) Sharif, S.; Denisov, G. S.; Toney, M. D.; Limbach, H. H. *J. Am. Chem. Soc.* **2006**, *128*, 3375−3387.

C. The Roles of Active-Site Residues in AlaR Catalysis. The AlaR active site is located in a cleft between two subunits (Figures 1 and 5), deeply embedded within the protein. The PLP cofactor is bound by a network of hydrogen bonds plus hydrophobic interactions (Tables 4 and 5). Arg219 bridges between His166 and the pyridine nitrogen (N1) of PLP. His166, in turn, interacts with Tyr265′ to hold the phenolate ion in position for the proton abstraction reaction. The interaction between N1 and Arg219 makes it virtually impossible for the pyridine ring to be protonated. This was first described by Ringe and co-workers by examining the X-ray crystal structures[17,18] and was subsequently confirmed by spectroscopic studies of the reaction mechanism.[9] Mutation of Arg219 to Glu greatly reduces the racemase activity and introduces transamination activity.[73] Interestingly, this mutation gives a local structure analogous to typical PLP-dependent enzymes, where the N1 position is protonated, favoring the formation of a quinonoid intermediate.[9,73] Arg136 forms hydrogen-bonding bridges with the anionic O3A atom of the cofactor and the carboxylate group of the substrate. The carboxylate group of the substrate also interacts with the backbone amide of Met312′. Lys39 forms an ion-pair with Asp313′. The phosphate group of PLP is hydrogen-bound to Tyr43, Asn203, Ser204, Tyr354, and the backbone amides of Ser204, Gly221, and Ile222. It is interesting to note that, on either side of the PLP-pyridine ring, there exists a continuous path of hydrogen-bonded water molecules extending to the protein surface.

The specific roles of active-site residues, important to binding and to catalysis, are probed by an interaction energy decomposition analysis, a procedure that involves sequential charge-annihilation to determine the average interaction energies, starting from the amino acids closest to the active site. This approach was first used by Bash et al. in the study of triosephosphate isomerase,[74] and it has been applied to a number of enzyme systems.[75,76] Although the energy decomposition analysis depends on the division of QM and MM regions, the results can still provide important information on binding interactions and transition-state stabilization. Below, we briefly describe the computational procedure before discussing the results.

We used the structures saved during the umbrella-sampling MD simulations, corresponding to the reactant state (R), transition state (TS), and product state (P), within a range of 0.1 Å of the reaction coordinate stationary points. These three states are defined by R_C^1 at −1.0, 0.2, and 1.5 Å and R_C^2 at −1.25, 0.2, and 1.25 Å, respectively. A total of 750 configurations were averaged for each of the R, TS, and P states. For each configuration, we sequentially zeroed the MM charges of one amino acid residue roughly in order of the distance between the C_α of the residue and the center of the substrate. Initially, the QM energy of the fully charged system was determined. Subsequently, at each step of charge deletion of residue *I*, the QM energy was determined after the charge annihilation, and the energy difference corresponds to the interaction energy between this residue and the QM subsystem:

$$\Delta E(I) = [E_{QM} + E_{QM/MM}] - [E_{QM}(I) + E_{QM/MM}(I)] \quad (5)$$

where $E_{QM}(I)$ and $E_{QM/MM}(I)$ are the QM and QM/MM energies computed when the MM charges of residue *I* have been annihilated. The results are then averaged. Since the most interesting quantity is the change in the interaction energies on going from the R to the TS and to the P state, we have computed this difference in Figure 6 for the proton abstraction of L-Ala-PLP by Tyr265′, and in Figure 7 for the proton abstraction of D-Ala-PLP by Lys39. In the latter case, the R state corresponds to neutral Lys39 abstracting H_α from D-Ala-PLP, while the P state is the carbonanion intermediate.

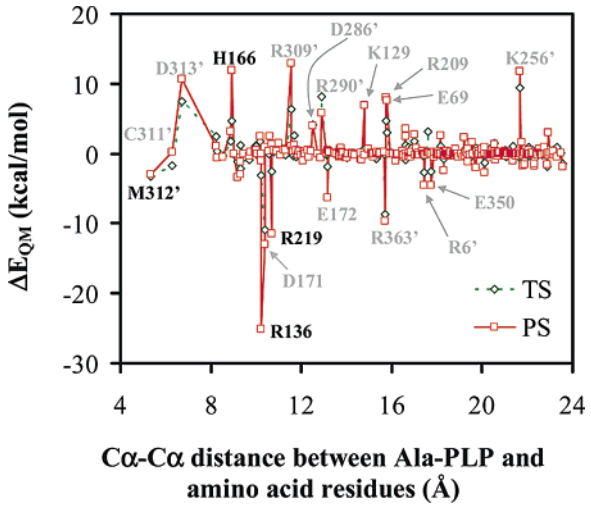

Figure 6. Individual residue contributions to stabilization or destabilization of the transition state (dotted green line) and the product state (solid red line) relative to the reactant state (the L-Ala-PLP Michaelis complex in alanine racemase) as a function of the distance between the C_α atoms of L-Ala-PLP and residues. Residues marked by a prime correspond to those in subunit B. Residue names in black indicate those that form hydrogen-bonding interactions with the Ala-PLP moiety, Tyr265′, and Lys39. Residues shown in gray do not have direct contact with the QM region.

Both Arg219 and Arg136 form strong hydrogen-bonding interactions with the external aldimine substrate. Arg219 donates a hydrogen bond to the pyridine nitrogen (N1) at an average distance of about 2.5 Å along the entire reaction path (Table 4). Furthermore, Arg219 provides stabilizing contributions to the TS by 3 kcal/mol relative to that at the Michaelis complex state, and this is enhanced to 12 kcal/mol in the product (deprotonation intermediate) state due to the accumulation of a negative charge as a result of the proton abstraction reaction (Figure 6). Arg136 involves multiple hydrogen-bonding (ion-pair) interactions with the external aldimine, including the oxyanion (O3A) of PLP and the carboxylate group (OXT) of the substrate (Figure 5, Chart 2). The average distances to O3A gradually decrease as the proton abstraction occurs (Table 4), also due to enhanced electrostatic attraction, which is reflected in the computed interaction energies that stabilize the TS by 3 kcal/mol and the product state by 25 kcal/mol over the Michaelis complex.

His166 plays a key role in positioning the catalytic base Tyr265′ for the proton abstraction reaction, which also contributes to stabilization of the phenoxide anion by lowering the pK_a of Tyr265′ to 7.3.[9] His166 is bridged between Arg219 and Tyr265′ with interaction distances of about 2.9 Å for both

(73) Yow, G.-K.; Watanabe, A.; Yoshimura, T.; Esaki, N. *J. Mol. Catal. B* **2003**, *23*, 311−319.
(74) Bash, P. A.; Field, M. J.; Davenport, R. C.; Petsko, G. A.; Ringe, D.; Karplus, M. *Biochemistry* **1991**, *30*, 5826−5832.
(75) Garcia-Viloca, M.; Truhlar, D. G.; Gao, J. *Biochemistry* **2003**, *42*, 13558−13575.
(76) Hensen, C.; Hermann, J. C.; Nam, K.; Ma, S.; Gao, J.; Höltje, H. D. *J. Med. Chem.* **2004**, *47*, 6673−6680.

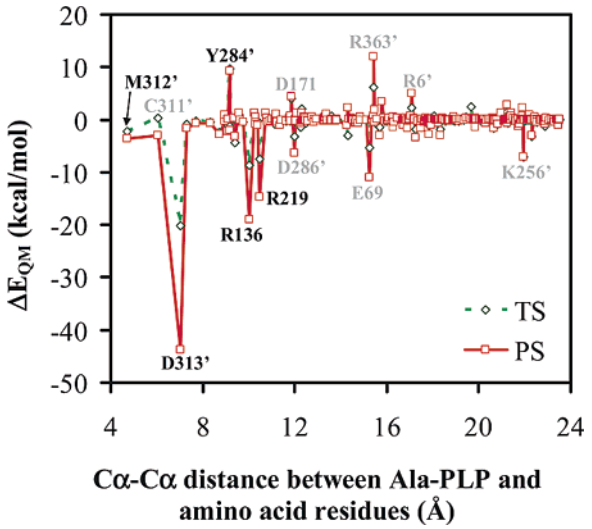

Figure 7. Individual amino acid residue energy contributions to the transition state (dotted green line) and product state (solid red line) relative to the reactant state as a function of the distance between the C_α atoms of D-Ala-PLP and AlaR amino acid residues. Residues marked by a prime correspond to those in subunit B. Residue names in black indicate those that form hydrogen-bonding interactions with the Ala-PLP moiety, Tyr265′, and Lys39. Residues shown in gray do not have direct contact with the QM region.

Chart 2. Atom Types for Pyridoxal Phosphate Coupled to Alanine (Ala-PLP) via a Schiff Base

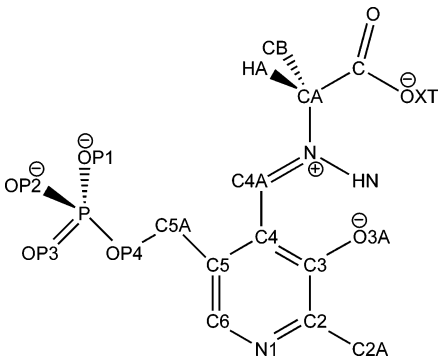

hydrogen bonds, which are increased to about 3.1 Å in the intermediate state (Table 4). Energy decomposition analyses show that His166 contributes negatively to catalysis, destabilizing the TS by 5 kcal/mol, which underscores the structural role of His166 in catalysis. Tyr265′ is additionally stabilized by a crystal water molecule (Wat-f in ref 16), which forms hydrogen bonds with both Tyr265′ and the PLP phosphate group (Table 4 and Chart 2).

Met312′ stabilizes both the transition state and the reaction intermediate (P) by 3 kcal/mol relative to the reactant state (Figure 6). The backbone amide group of Met312′ donates a hydrogen bond to the carboxylate group of the substrate, and the average distance is slightly shortened at the transition state (Table 4). Asp313′ forms an ion-pair with the acidic residue Lys39, which is in turn ion-paired with the carboxylate group of the substrate. The presence of a negative charge in close proximity to the PLP cofactor results in destabilizing contributions to the TS and P state by 7 and 11 kcal/mol, respectively.

In addition to the specific hydrogen-bonding interactions highlighted above, we can also identify a pattern of global electrostatic effects that affects the deprotonation reaction. A number of residues stabilize the transition state and the deprotonation intermediate but are not in close proximity to the substrate and the catalytic base Tyr265′. If we divide the active site by the molecular plane of the substrate aldimine moiety, we find that negatively charged residues that stabilize the transition and product states, including Asp171, Glu172, and Glu350, are located on the side where the α-proton is abstracted (Tyr265′ side) and that Arg6′ and R363′, which provide stabilizing contributions to the TS, are located on the opposite side of the PLP cofactor (Lys39 side). Conversely, residues Glu69, Asp286′, and Asp313′ are located on the reprotonation (Lys39) side, and they destabilize the transition state of the proton abstraction by Tyr265′. The positively charged, destabilizing residues, including Arg209, Lys256′, Arg290, and Arg309′, are situated on the deprotonation (Tyr265′) side. This global pattern is consistent with the direction of charge migration in the proton-transfer reaction, bringing a net positive charge to the Tyr265′ side of the active site, which thus is stabilized by negatively charged residues and destabilized by positively charged residues on this side of the pseudoplane of the cofactor. As the deprotonation intermediate develops an additional negative charge following the proton-transfer reaction, positively charged residues are favored on the reprotonation (Lys39) side.

For the second, reprotonation step in the L-to-D conversion, the reverse process is equivalent to the proton abstraction of D-Ala-PLP by a neutral Lys39 in the D-to-L conversion. In the following, we have presented the results and discussion of this reaction step in the direction corresponding to the D-to-L conversion. Asp313′ has the greatest effects on transition state and deprotonation intermediate state stabilization, contributing 19 and 44 kcal/mol, respectively. This is clearly due to the formation of an ion-pair between the two residues as Lys39 gains a proton in the chemical step. The enhanced interactions are reflected by a concomitant decrease in hydrogen-bonding distances from 2.83 to 2.58 Å. As in the L→D conversion, Arg136 stabilizes the TS and the intermediate state by 9 and 19 kcal/mol, respectively, whereas Arg219 favors these two states by 6 and 13 kcal/mol. These effects are also reflected in the distances of the hydrogen bonds that involve Arg219 and Arg136 (Table 5). Tyr284′ makes destabilizing contributions to the transition state, although it is not directly hydrogen-bonded to the QM region. Additional residues that are not in direct contact with the QM region but make noticeable contributions are the charged residues enumerated above for the L-to-D reaction. The global features of the electrostatic interactions remain the same in the reverse isomerization, but the roles of these charged residues are reversed as well. Thus, Glu69, Lys256′, and Asp286′ make TS-stabilizing contributions, whereas Arg6′, Asp171′, and Arg363′ have destabilizing effects.

The role of some of these residues may be tested by mutagenesis experiments. To date, mutational experiments have focused on active-site residues in direct contact with Ala-PLP.[9,11,12,73,77−79] Sun and Toney studied the role of Arg219 in catalysis by mutants R219K, R219A, and R219E and found that a positively charged residue is essential at this position, due to stabilization of the catalytic residue Tyr265′ via His166.[9]

(77) Kurokawa, Y.; Watanabe, A.; Yoshimura, T.; Esaki, N.; Soda, K. *J. Biochem.* **1998**, *124*, 1163−1169.
(78) Seebeck, F. P.; Hilvert, D. *J. Am. Chem. Soc.* **2003**, *125*, 10158−10159.
(79) Fenn, T. D.; Holyoak, T.; Stamper, G. F.; Ringe, D. *Biochemistry* **2005**, *44*, 5317−5327.

Table 6. Computed and Experimental Kinetic Isotope Effects for the Deprotonation of L-Ala by Alanine Racemase[a]

L→D			D→L		
BQCP	VTST/MT	expt[a]	BQCP	VTST/MT	expt[a]
4.21	3.97	1.93 ± 0.13	3.06	2.65	1.43 ± 0.20

[a] Reference 14.

Wantanabe et al. found that the Y265F mutant reduces the racemization activity 1600-fold,[11,12] and they further studied the K39A mutant and concluded that Lys39 participates directly in catalysis,[10,77] finding that K39A activity may be rescued by addition of methylamine. Moreover, Yow et al. found that mutation of both Tyr265′ and Lys39 in AlaR abolished any racemase activity but increased the transaminase activity by 6.6-fold.[73] Seebeck and Hilvert found that mutation of Tyr265′ to Ala considerably increased the aldolase activity of AlaR,[78] while Ringe and co-workers studied the Y265F mutant effect on the suicide inhibitor cycloserine inactivation of AlaR.[79] In light of the results presented herein, mutagenesis of additional residues not in direct contact with the substrate might be of interest.

D. Kinetic Isotope Effects. The quantum mechanical potentials of mean force are displayed in Figure 4, which incorporate the QM corrections to the classical PMF from MD simulations. In this section, we further analyze the QM effects in the alanine racemase reaction by computing the primary kinetic isotope effects for the proton-transfer reactions. We employed two computational approaches to include the QM correction: the first is based on the quantized classical path method with bisection sampling (BQCP) described previously,[50,51] and the second makes use of the ensemble-averaged variational transition-state theory with multidimensional tunneling (EA-VTST/MT).[52] In the former approach, both zero-point effects and tunneling are included, whereas the EA-VTST/MT provides a procedure that approximately separates these two factors to gain further insight into the QM contributions in enzyme reactions. The agreement, as we see below, between these two entirely different methods provides further support for the computational results.

For the L- to D-alanine racemization in AlaR, the first step in the proton abstraction by Tyr265′ is rate-limiting, and thus the observed rate constant is directly related to this reaction step, $k_{obs} = k_1$ (Scheme 1). In the bisection PI simulation method, we quantize the donor and acceptor heavy atoms along with the transferring proton by representing each atom with 32 beads. The centroid positions of these beads are constrained to coincide with the corresponding "classical" positions from MD simulations. The quantized beads are sampled exactly on the basis of free particle distributions.[50,51] Furthermore, we have implemented a perturbation approach[58] which allows sampling of the isotopic beads distributions proportional to the ratio of the de Broglie wavelength in the bisection sampling scheme, achieving the required accuracy for computing KIEs. As already discussed above, inclusion of QM contributions to the computed classical PMF (Figure 4) lowers the free energy barrier by 2.60 and 1.74 kcal/mol respectively for proton and deuteron transfer to the Tyr265′ phenolate ion. This leads to a computed intrinsic KIE of 4.21 for the α-proton abstraction in the L- to D-alanine conversion (Table 6). The computational result is greater than the experimental value of 1.9,[14] and the origin of the discrepancy is not exactly clear, although several factors may be involved, including the complexity involved in the analysis of experimental kinetic data, the possibility that the experimental KIE was not exactly the intrinsic value, and computational uncertainty.

To provide additional insight into the quantum mechanical effects, we also computed the QM correction to the classical PMF by using the EA-VTST/MT approach. In addition, we have estimated the dynamic recrossing transmission coefficient with the method described in ref 52. In the EA-VTST/MT method, the computation was divided into two stages. In the first stage, we quantized the nuclear vibrations for the QM subsystem by determining the instantaneous normal modes to obtain a quasiclassical PMF, $\Delta G^{qc}(R_C^1)$. In this stage, the degree of freedom, corresponding to the reaction coordinate R_C^1, was projected out before computing the instantaneous normal modes. Thus, tunneling is not included in $\Delta G^{qc}(R_C^1)$, which is subsequently included in the total rate constant by determining the tunneling transmission coefficient using the optimized multidimensional tunneling algorithm developed by Truhlar and co-workers (for a recent review, see ref 60). Although this separation of QM effects is not exact, it does provide reasonable insight into the relative effects of zero-point energies and QM tunneling for the proton-transfer reaction. In the case of the AlaR reaction, we found that the dominant QM contribution is due to the change in zero-point energy on going from the reactant state to the transition state and that hydrogen tunneling is negligible, with an average transmission factor of 1.14 and 1.31 for the hydrogen and deuterium (Table 7), respectively, in the step performed by Tyr265′. In addition, we found that the average recrossing transmission factors, Γ, are close to unity, with values of 0.96 and 0.94 for the hydrogen and deuterium transfers, respectively (Table 7). Combining the classical and quantum transmission coefficients along with the bound vibrational quantum contributions, the computed intrinsic KIE is 3.97 for the Tyr265′ proton abstraction (Table 6), which is in close agreement with the PI simulation results. Finally, we note that the net quantum effects from EA-VTST/MT calculations lower the classical barrier by 2.71 and 1.89 kcal/mol respectively for the hydrogen- and deuterium-transfer reactions, also in accord with the BQCP calculations.

For the D→L conversion of alanine by AlaR, if we neglect the complexity of reaction steps involving internal and external aldimine exchange, substrate binding, and product release, i.e., we consider only the proton abstraction and reprotonation steps, the overall rate constant for the "chemical step" can be expressed as follows:

$$k_{eff} = \frac{k_{-2}k_{-1}}{k_{-1} + k_2} \tag{6}$$

Since our simulations show that $k_2 \gg k_{-1}$, we obtain the following rate expression:

$$k_{eff} = \frac{k_{-2}k_{-1}}{k_2} = \frac{k_{-1}}{K_2} \tag{7}$$

where K_2 is the equilibrium constant for the proton transfer from L-Ala-PLP to a neutral Lys39. On the basis of the relative free energies for different reaction steps in Figure 4, we obtained an estimated primary KIE of 3.06 from PI simulations and 2.65 from EA-VTST/MT. If we consider the intrinsic KIE of the

Table 7. Average Computed Transmission Coefficients for the Protio and Deuterio Isotopes for the Deprotonation of L-Ala by Alanine Racemase[a]

	L→D			D→L		
isotope	$\langle\Gamma(T)\rangle$	$\langle\kappa(T)\rangle$	$\langle\gamma(T)\rangle^b$	$\langle\Gamma(T)\rangle$	$\langle\kappa(T)\rangle$	$\langle\gamma(T)\rangle^b$
H	0.96 ± 0.06	1.14 ± 0.16	1.07 ± 0.15	0.81 ± 0.15	1.05 ± 0.10	0.86 ± 0.20
D	0.94 ± 0.05	1.31 ± 0.25	1.20 ± 0.21	0.87 ± 0.12	1.09 ± 0.16	0.97 ± 0.24

[a] The transmission coefficients were computed as the average over 10 protein configurations using the static secondary zone approximation. [b] $\langle\gamma(T)\rangle = \langle\Gamma_i(T)\,\kappa_i(T)\rangle_i$.

initial proton abstraction from D-Ala by Lys39 to yield the intermediate, BQCP predicts a value of 4.60, while EA-VTST/MT gives a value of 3.33. Both values are greater than that obtained by multicomponent analyses of experimental kinetic data, which yielded a value of 1.43 ± 0.20.[14] It is worth noting that an earlier study that utilized the Lys39Ala mutant showed a greater primary KIE of 5.4, in which a small molecule, methylamine, was proposed to act as an enzyme-rescuing agent.[10] In closing this section, we note that the computed recrossing transmission coefficients are 0.81 and 0.87 respectively for the proton and deuteron transfers to Lys39, which are somewhat smaller than those of the L-to-D isomerization, but they are still very close to unity.

Conclusions

We have carried out a mixed quantum and classical simulation study of the alanine racemase reaction by using a combined QM/MM potential to describe the bond-making and bond-breaking processes and a centroid path integral method to incorporate nuclear quantum corrections. Alanine racemase is a pyridoxal 5′-phosphate-dependent enzyme, but its active site has a unique feature, in that the pyridine nitrogen of the cofactor is unprotonated because it accepts a hydrogen bond from Arg219. This structural feature makes it difficult to form a charge-delocalized quinonoid intermediate as in other PLP-dependent enzymes, yet AlaR can still effectively lower the α-amino carbon acidity and enhance the reaction rate of the rate-limiting proton-transfer reactions. In this work, we have identified that the mechanisms of carbon acidity enhancement by a pyridine-protonated PLP and an unprotonated PLP are different. Consistent with previous proposals, the "normal" Ala-PLP (pyridine-protonated form) aldimine adduct increases the α-carbon acidity by a combination of factors of the neighboring iminium ion moiety[19] and charge delocalization to form a quinonoid intermediate. On the other hand, the pyridine-unprotonated Ala-PLP species lowers the aqueous pK_a by stronger solvation stabilization of the carbanion conjugated base. The enzyme AlaR provides additional stabilization of the conjugated base, making it feasible to have a proton-transfer from a carbon acid to a relatively weak base (Tyr265′ or Lys39).

The second key finding of this study is that the mechanism of racemization of an alanine zwitterion in water is altered from an essentially concerted process to a stepwise reaction by formation of an external aldimine adduct with the PLP cofactor. The aldimine adduct lowers the pK_a of the carbon acid of alanine by forming a "carbanion" intermediate, stabilized either by formation of a quinonoid species or by solvent effects. The enzyme further lowers the free energy barrier of the proton-transfer reactions in the racemization process, and this is achieved through a combination of specific hydrogen-bonding interactions with amino acid residues in direct contact with the external aldimine adduct and distant electrostatic interactions that favors charge separation in the proton-transfer reaction.

Finally, we have computed the primary kinetic isotope effects for the proton abstraction of L-Ala-PLP external aldimine by Tyr265′ and for the reprotonation of the carbanion intermediate by Lys39. The computed intrinsic KIEs are greater than the values derived from experimental rate constants, but the latter results may reflect the difficulty in extracting intrinsic KIEs due to kinetic complexity of the enzymatic reaction cycle, involving a series of reaction steps that have similar barrier heights. Importantly, we found that the classical free energy barriers for the two proton-transfer reactions are lowered by about 3 kcal/mol when nuclear quantum mechanical effects are included. Analyses of the origin of the quantum effects using ensemble-averaged variational transition-state theory with multidimensional tunneling show that the dominant factor is from the change in zero-point energies from the reactant state to the transition state. Quantum mechanical tunneling makes only minor contributions to the barrier reduction. These findings are in accord with studies of other enzymes.

Acknowledgment. This work has been supported by the National Institutes of Health. We thank Professor Darrin York for making his optimization program available in this study.

Supporting Information Available: Tables of SRP-AM1 parameters; tables of energies, geometries, and electronic properties for parametrized molecules; quantum corrections plots from instantaneous normal-mode analysis; and complete refs 39 and 41. This material is available free of charge via the Internet at http://pubs.acs.org.

JA066334R